Chinese Journal of Chemical Engineering 28 (2020) 889–895

Contents lists available at ScienceDirect

Chinese Journal of Chemical Engineering

journal homepage: www.elsevier.com/locate/CJChE

Article

Interfacial potassium induced enhanced Raman spectroscopy for single-crystal TiO_2 nanowhisker

Fan Pan [1], Guobing Zhou [2], Liangliang Huang [2], Wei Li [3], Mingshen Lin [4], Chang Liu [1,*]

[1] State Key Laboratory of Materials-Oriented Chemical Engineering, Nanjing Tech University, Nanjing 210009, China
[2] School of Chemical, Biological & Materials Engineering, University of Oklahoma, Norman, 73019, United States
[3] European Bioenergy Research Institute and Aston Institute of Materials Research, Aston University, Birmingham B4 7ET, United Kingdom
[4] TA Instruments-Waters LLC, Shanghai 200233, China

ARTICLE INFO

Article history:
Received 14 July 2019
Received in revised form 10 September 2019
Accepted 17 October 2019
Available online 25 October 2019

Keywords:
TiO_2 nanowhisker
SERS
potassium induced

ABSTRACT

Structural control and element doping are two popular strategies to produce semiconductors with surface enhanced Raman spectroscopy (SERS) properties. For TiO_2 based SERS substrates, maintaining a good crystallinity is critical to achieve excellent Raman scattering. At elevated temperatures (>600 °C), the phase transition from anatase to rutile TiO_2 could result in a poor SERS performance. In this work, we report the successful synthesis of TiO_2 nanowhiskers with excellent SERS properties. The enhancement factor, an index of SERS performance, is 4.96×10^6 for methylene blue molecule detecting, with a detection sensitivity around 10^{-7} mol·L^{-1}. Characterizations, such as XRD, Raman, TEM, UV–vis and Zeta potential measurement, have been performed to decrypt structural and chemical characteristics of the newly synthesized TiO_2 nanowhiskers. The photo absorption onset of MB adsorbed TiO_2 nanowhiskers was similar to that of bare TiO_2 nanowhiskers. In addition, no new band was observed from the UV–vis of MB modified TiO_2 nanowhiskers. Both results suggest that the high enhancement factor cannot be explained by the charge-transfer mechanism. With the support of *ab initio* density functional theory calculations, we reveal that interfacial potassium is critical to maintain thermal stability of the anatase phase up to 900 °C. In addition, the deposition of potassium results in a negatively charged TiO_2 nanowhisker surface, which favors specific adsorption of methylene blue molecules and significantly improves SERS performance *via* the electrostatic adsorption effect.

1. Introduction

Surface-enhanced Raman spectroscopy (SERS) is one of the most sensitive spectroscopic techniques to detect molecules that have a strong Raman response at a single-molecule resolution [1]. In recent years, TiO_2 semiconductor-based SERS has attracted much attention due to the advantages of low cost, good stability and excellent reproducibility [2–4]. TiO_2 SERS performance is mainly tuned *via* the preparation protocol where element doping (hydrogen and oxygen), morphology manipulation and band structure engineering are beneficial. Compared with traditional coinage metal substrates such as gold, silver and copper, TiO_2 photocatalytic properties enable an environment-friendly removal of adsorbed molecules and a reuse of the SERS substrate [5].

Despite the promise, semiconductor-based SERS substrates are generally limited by the inferior enhancement factor (EF), an index of how sensitive the detection is. The theoretical maximum EF for semiconductor-based SERS [4], based on charge-transfer (CT) mechanism, has been estimated to be around 10^6. However, reported experimental EF values for TiO_2 substrates are only in the range of 10 - 10^3. Generally, there are two options to improve the SERS performance. The first one is to change the semiconductor morphology and thus enhance the interactions between the laser and the substrate. Under this guideline, Alessandri synthesized TiO_2 shell-based spherical resonators and reported a remarkable Raman scattering enhancement [6]. The improvement is ascribed to the synergistic effects of high refractive index of TiO_2 shell layer and multiple light scattering through spherical geometries. Similarly, Zhang and co-workers used a sol–gel method and prepared TiO_2 inverse opal photonic microarrays [7]. They reported that the morphology change results in the photonic band gap change, which in return promotes multiple light scattering and the resulted EF is about 10^4. Recently, we adopted a two-step anodic oxidation process and prepared TiO_2 nanofoam–nanotube array [8], which shows a remarkable Raman scattering enhancement for methylene blue ($EF = 2.3 \times 10^5$). The second option is to manipulate interactions between the substrate and adsorbed molecules. For example, Cong and co-workers engineered oxygen vacancy at tungsten oxide nanowire surfaces [9]. It was observed that the new interfacial oxygen vacancies can enrich tungsten oxide surface states, strengthen adsorbent–adsorbate interactions, and eventually produce an improved EF value of 3.4

* Corresponding author.
E-mail address: changliu@njtech.edu.cn (C. Liu).

https://doi.org/10.1016/j.cjche.2019.10.003
1004-9541/

$\times 10^5$. Inspired by Cong's work, hydrogen or oxygen doping has been adopted to treat other semiconductors [5]. It is generally accepted that quasi-amorphous interfacial thin layers and hydrogen or oxygen doping effectively facilitate charge transfer, enhance vibrational scattering of adsorbed molecules and improve the SERS performance.

It is worth pointing out that defect engineering is a double-edged sword. A poorly designed defective interface can severely degrade SERS performance. For example, it was reported that the excess amorphous structure at interface can decrease the refractive index, which could weaken the interactions between the SERS substrate and the laser [4]. Also, interfacial defects can induce the transformation and re-combination of electron/hole pairs, which will degrade SERS performance [10]. For instance, Zhao and co-workers investigated the crystallinity effect of anatase TiO_2 nanoparticles on SERS performance [11]. They concluded that both high degree of crystallinity and high concentration of surface defects are critical for a superior SERS performance. However, the challenge is that the two factors do not come together very easily for TiO_2 materials: using a high-temperature treatment (normally above 600 °C) to improve anatase TiO_2 crystallinity, one can easily witness the intrinsic phase transformation from anatase to rutile TiO_2. The as-synthesized TiO_2 substrate has an inferior SERS performance.

In this work, we report a new semiconductor SERS substrate-TiO_2 nanowhisker with high crystallinity and high thermal stability. The single anatase crystal phase remains intact up to 900 °C, which is mainly due to the interfacial potassium. In addition, potassium binds strongly with TiO_2 substrate, producing a negatively charged interface for Raman scattering, as well as altering the band gap of anatase TiO_2. All three factors, namely, the single-phase crystallinity, the negatively charged interface and the reduced band gap, synergistically enable the synthesized anatase TiO_2 nanowhisker to be a supreme SERS substrate, with a maximum EF 4.96×10^6. The significance of this work is two-fold: the report of a new SERS performance record from TiO_2 semiconductor, and the exploration of interfacial potassium doping effect. We anticipate other alkali elements can also assist engineering TiO_2 materials to achieve high crystallinity, high thermo stability and high interaction selectivity.

2. Experimental

2.1. Materials

Metatitanic acid ($TiO_2 \cdot nH_2O$) was from Nanjing oil chemicals Co., Ltd., China. Potassium carbonate (K_2CO_3) was from Shanghai chemical reagent factory. Methylene blue (MB) was purchased from Tianjin Chemical Reagent Research Institute Co., Ltd. All chemicals were of analytical grade and used as received. Deionized water was used in all experiments.

2.2. TiO_2 nanowhisker synthesis

TiO_2 nanowhisker was synthesized by a two-step calcination and ion exchange process, as illustrated in Fig. 1 [12]. Briefly, metatitanic acid ($TiO_2 \cdot nH_2O$) and potassium carbonate were mixed with a 1.9 mol·L^{-1} ratio. The mixture was then calcined in the muffle furnace at 820 °C for 6 h. After that, the as-obtained potassium dititanate was washed with 0.1 mol·L^{-1} HCl and deionized water, repeating for three times. Finally, the TiO_2 nanowhiskers were obtained by calcinating the powders at different temperatures for 2 h. According to the temperature used in the final calcination step, obtained TiO_2 samples were named as Z700, Z800, Z900 and Z1000, respectively.

2.3. Characterizations

The crystal structures of those samples were characterized by X-ray diffraction (XRD, Bruker, Model D8 with Cu Kα excitation). In addition, the element composition and chemical states of studied samples were analyzed by X-ray photoelectron spectrometer (XPS, Physical Electronics 5600). The UV–vis diffuse reflectance spectra (UV–vis DRS) was obtained by a UV–vis spectrometer (Perkin-Elmer Lambda 950) over a wavelength range of 300-800 nm. Surface morphologies were studied by using field-emission scanning electron microscope (FESEM, Hitachi S-4800) at 5 kV, 10 μA. Surface charge of the samples were detected on the Zeta potential analyzer (Malvern, ZS90). TEM images were obtained employing JEM-2010 UHR at 200 kV.

2.4. SERS measurement

The Raman signal of MB molecules adsorbed on TiO_2 nanowhiskers were obtained using the 514.5 nm laser excitation. Specifically, we obtain the 10^{-5} mol·L^{-1} MB ethanol solution by successively diluting a 10^{-3} mol·L^{-1} MB solution. Then 20 μl of the 10^{-5} mol·L^{-1} MB ethanol solution was added to TiO_2 substrate, keeping the sample in the dark for 4 h to reach the adsorption equilibrium. Subsequently, the Raman spectra were collected *via* the high-resolution confocal Raman spectrometer (LabRAM HR-800) using a 50 × LWD objective lens for 10 s and 0.3 mW powers in all acquisitions. Each sample was collected at least 5 times from different locations of the sample.

3. Results and Discussion

3.1. The characterization of TiO_2 nanowhisker

As shown in Fig. 2a, scanning electron microscopy (SEM) images demonstrate that the four samples possess one-dimensional morphology. For the Z700 sample, the diameter is about 300 nm and the length is a few microns. When the temperature increases from 700 °C to 1000 °C, all studied samples shrink a little bit and their diameters increase slightly. This indicates that TiO_2 nanowhisker could melt partially at high temperatures. According to XRD characterizations in Fig. 2b, Z700 and Z800 are pure anatase crystalline phase, while Z900 and Z1000 have a small portion of rutile crystalline phase. The content of rutile phase was estimated to be 2 mol% and 10 mol% for Z900 and Z1000, respectively [13]. TEM images of those nanowhiskers are available in Fig. S2, where a crystal phase of nanowhiskers was measured, consistent with XRD results.

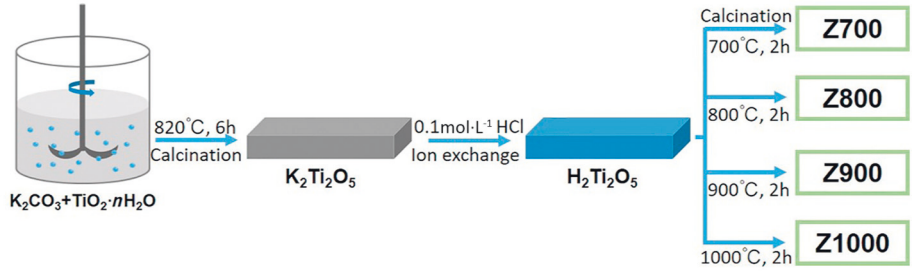

Fig. 1. Schematic diagram of TiO_2 nanowhisker preparation.

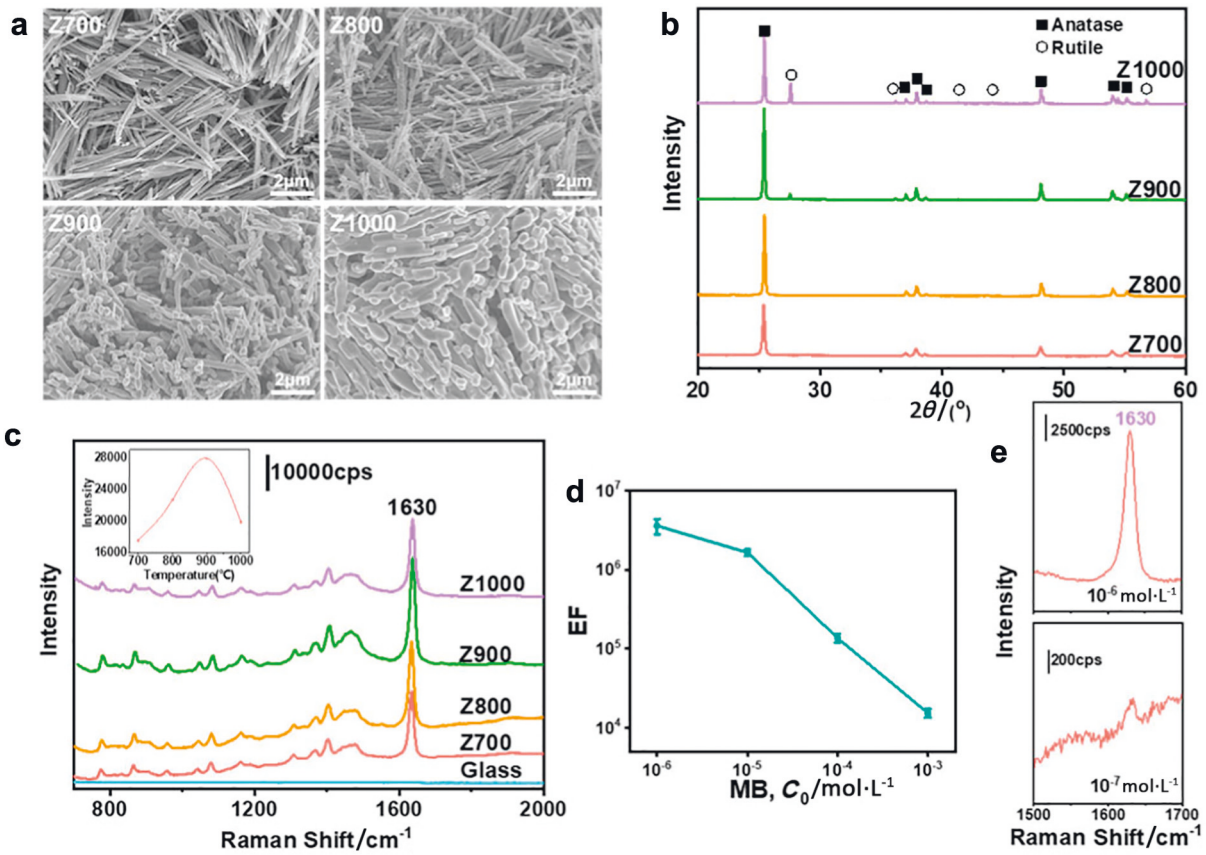

Fig. 2. Morphology, crystal structure and SERS properties of four TiO_2 nanowhisker samples. (a) SEM images of Z700, Z800, Z900 and Z1000. (b) XRD pattern of four TiO_2 nanowhiskers. (c) Raman spectra of the 10^{-5} mol·L^{-1} MB ethanol solution on four TiO_2 nanowhiskers and bare glass (inset: the 1630 cm^{-1} intensity of four nanowhiskers). (d) Raman EFs obtained for MB on the Z900 sample, as a function of MB concentrations at the 1630 cm^{-1} peak. (e) The detection limitation test of MB on the Z900 sample.

3.2. SERS properties of TiO_2 nanowhisker samples

Methylene blue (MB) was used as the probe molecule to examine the SERS performance of TiO_2 nanowhiskers. As shown in Fig. 2c, the SERS enhancement factor (EF) is calculated at the characteristic peak of 1630 cm^{-1}, which is the aromatic C—C stretching vibration mode [9]:

$$EF = (I_{SERS}/N_{SERS})/(I_{bulk}/N_{bulk}) \quad (1)$$

where I_{SERS} and I_{bulk} refer to peak intensities of the SERS and non-SERS spectra, respectively. N_{SERS} and N_{bulk} correspond to the number of probe molecules in the laser area for the SERS and non-SERS measurements. Calculation details are available in the Section S2 of Supporting Information.

Significant SERS enhancements are observed for all four samples but there is almost no enhancement from the bare glass substrate. The Z900 sample shows the best SERS performance compared with other samples. It is probably because Z900 has a high crystallinity. It is worth pointing out that when the calcination temperature increases to 1000 °C, a significant phase transformation will occur, from the anatase to rutile phase, which will result in a decrease of Raman detecting signal of MB molecules. The trend of anatase phase has a better SERS performance than the rutile phase is also reported by Zhao *et al.* [14]. As illustrated in Fig. 2d, the calculated EF from the Z900 sample is 4.96×10^6 at the 10^{-6} mol·L^{-1} MB concentration, which is the best performance reported so far for TiO_2-based SERS substrates (Table S1). In addition, the Z900 sample has an applicable detection of MB molecules even at a very dilute concentration of 10^{-7} mol·L^{-1}, see Fig. 2e. Such detecting sensitivity is better than most reported results from semiconductor SERS substrates.

3.3. TiO_2 morphology and SERS performance

TiO_2 SERS substrates are traditionally polycrystalline materials, with the morphology of nanoparticles or mesoporous membranes. The TiO_2 nanowhisker synthesized in this work is a one-dimensional single crystal. A high crystallinity could improve the SERS performance. For example, Sun and co-workers reported that one-dimensional semiconductor materials with single crystal structures (such as nanowire and nanobelt), are excellent plasmonic waveguides to transfer Raman signals and realize remote SERS properties [15]. Such signal transfer and remote Raman scattering are promising for Raman scattering enhancement. For the Z700 sample, as shown in Fig. 3d and e, remote Raman scattering was also observed. In order to further validate the dominating contribution of the single crystal morphology, a new set of three samples has been prepared: Z700 nanowhisker with the one-dimensional morphology (Fig. 3a); ZB700, a sample from ball-milling Z700, where the single crystallinity was destroyed (Fig. 3b); T700, a mesoporous TiO_2 nanowhisker sample prepared with additional water vapor treatment during the Z700 sample preparation (Fig. 3c). The detailed preparation conditions are provided in the supporting information and see also Fig. S1. The key differences between three samples: ZB700 sample is composed of TiO_2 nanoparticles with irregular morphologies; T700 has the one-dimensional morphology, similar to that of Z700. But T700 has a significant number of cavities at the surface. SERS performances of the three samples are compared in Fig. 3f. First of all, the Raman scattering at low wavenumbers (200-800 cm^{-1}) supports that all three samples are generally composed of TiO_2 anatase phase. However, the SERS performance from the three samples is obviously different: at the characteristic 1630 cm^{-1} peak, the EF has the order of T700 < ZB700 < Z700 (Table S2). It is important to point out that despite the one-dimensional morphology, the cavities of T700

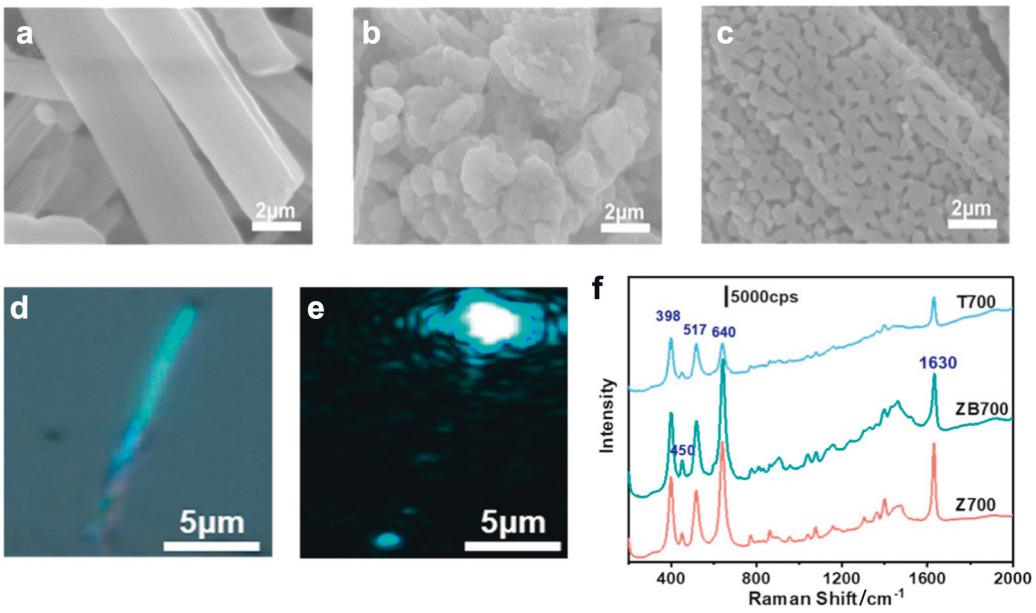

Fig. 3. Morphology, Remote SERS and SERS performance of TiO_2 samples. SEM images of Z700 (a), ZB700 (b) and T700(c). The propagation of light along TiO_2 nanowhisker (Z700) under visible light (d) and laser (e). (f) Raman spectra of MB (10^{-5} mol·L^{-1}) adsorbed on T700, ZB 700 and Z700 samples.

significantly degrade the SERS performance. In summary, both the single crystallinity and the one-dimensional morphology are important for excellent SERS performance.

3.4. Interfacial potassium and significant SERS improvement

Despite the performance degradation with respect to Z700 and ZB700, the T700 sample still has an EF of 4.13×10^5, higher than other reported TiO_2 semiconductors. Since T700 possesses no single crystallinity or perfect interfacial morphology, the excellent SERS performance is attributed by other factors. In literature, Zhao *et al.* reported that the photo absorption threshold to the 4-Mercaptobenzoic acid (4-MBA) adsorbed TiO_2 shows a blue-shift, compared with that of unmodified TiO_2. It is interpreted due to the interaction between adsorbed molecules and TiO_2 substrate [16]. Similarly, Cong *et al.* reported their X-ray photoelectron spectroscopy (XPS) results that hydrogen treated $W_{18}O_{49}$ sample has an increased percentage of W^{5+}, from 30.4 mol% (untreated, pristine $W_{18}O_{49}$) to 47.5 mol% [9]. Obviously, there are more surface oxygen vacancies of the modified sample. Moreover, they determined UV–vis diffuse reflectance spectroscopy (DRS) spectra of R6G molecules deposited on $W_{18}O_{49}$ and reported a new band from the hybrid sample, an evidence of the charge transfer between R6G and $W_{18}O_{49}$.

Inspired by those studies, UV–vis DRS and XPS were performed in this work to further explore the enhancement mechanism of Raman scattering. As shown in Fig. 4a, the photo absorption spectra for Z700, Z800 and Z900 samples are very similar to each other, with a same

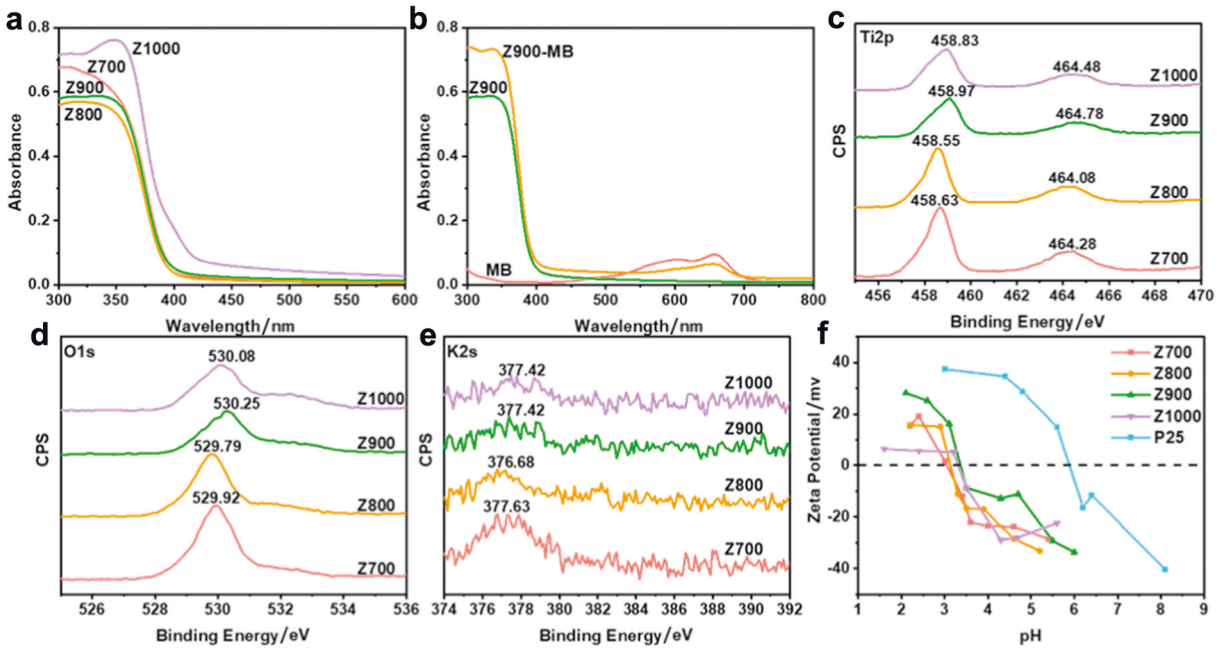

Fig. 4. UV–vis DRS spectra of (a) TiO_2 nanowhiskers and (b) Z900 compared with pristine Z900 and MB. XPS spectra and binding energies of (c) titanium, (d) oxygen and (e) potassium. (f) Zeta potential as a function of pH: the comparison between four studied TiO_2 nanowhiskers and the commercial P25 sample.

onset around 400 nm. Such result is in accordance with the photo absorption onset of TiO_2 anatase phase. A red shift of the absorption edge for Z1000 was observed, which is mainly due to the phase transformation and the resulted rutile phase. Ti2p and O1s peak positions of XPS spectra in Fig. 4c and d further confirmed that Z700 and Z800 are in the anatase phase, while Z900 and Z1000 have co-existing anatase and rutile phases [17]. Moreover, as shown in Fig. 4b, we compared UV–vis DRS spectra of MB molecule adsorbed on Z900 with that of pristine MB and Z900. No new band was observed from the spectra of MB modified Z900. In addition, the absorption edge of MB modified Z900 was same as that of the pristine Z900 sample. Those results suggested that the excellent SERS performance of TiO_2 nanowhisker is not from defect states near TiO_2 conduction band.

Generally, oxygen vacancy defects of TiO_2 nanoparticles can form surface state energy levels. Zhao *et al.* observed that defect states favor charge transfer between molecules and TiO_2 substrates. Also, the SERS signal is affected by temperature, which is ascribed to the improved crystallinity and the reduced concentration of surface defects [16]. In this work, the enhanced SERS performance is not dominated by oxygen vacancy defects. Firstly, the SERS signal of MB on Z800 is stronger than that of Z700, despite the fact that Z800 has a lower concentration of oxygen vacancy defects. Secondly, when calcination temperature increases, the XPS spectra peaks of Ti2p (Ti^{4+}, ~458.6 eV and 464.2 eV) and O1s (~529.9 eV) are expected to shift towards higher binding energies. However, the results in Fig. 4c and d show the opposite. It is worth noting, as suggested by Fig. 4e, that potassium remains at the interface and binds strongly with oxygen sites of studied samples. Although the trace of potassium is negligible to TiO_2 structural characterization, such as XRD results in Fig. 2b, the surface chemistry could have a drastic change due to the trace potassium at interface. The potassium bonded Ti sites could have higher electron densities, which subsequently promote charge transfer between MB and the TiO_2 substrate. For the Z800 sample, the amount of potassium was estimated to be around 0.5 wt% *via* XPS and X-ray fluorescence (XRF) experiments.

The Zeta potential measurement in Fig. 4f reveals that the point of zero charge (PZC) for studied TiO_2 nanowhiskers is in the range of pH 3.0 to 3.5, which is remarkably lower than that of the commercial P25 TiO_2 nanoparticles (~pH 6). Such PZC change indicates that the surface of TiO_2 nanowhisker is negatively charged, consequently interacting strongly with MB molecules through positive charged sites (see Fig. S4). The enhancement of electrostatic interactions is beneficial for SERS performance. We note that similar phenomenon has been reported on a Cu_2O SERS substrate [18]. In order to validate the effect of electrostatic interactions, two molecules with opposite charges, namely, crystal violet (CV) (+) and methyl orange (MO) (−), were used to study their SERS performances on Z700 sample. As shown in Fig. 5, the positively charged CV molecule shows a better SERS performance than the negatively charged MO molecule. See Table S3 of the Supporting Information for the calculated EFs. In conclusion, we contributed Raman scattering enhancement observed in this work to synergistic effects: the interfacial potassium induced charge transfer effect and the electrostatic adsorption effect due to surface negative charges of TiO_2 nanowhiskers.

To further verify the effect of interfacial potassium, we design a third set of experiments: use commercially available TiO_2 anatase particles (TP) with high purity (99.9%) and mix it with K_2CO_3 (purity 99%). The mixture was heated at 800 °C for 2 h to dope different concentrations of potassium. For the studied samples, "TP-0.14" denotes the TP sample with a content of 0.14 wt% potassium. As shown in Fig. 6, the TP-0.50 sample has the SERS performance of MB molecules. When the potassium content was increased to 2.45 wt%, new Raman peaks appear at 231, 285, 460 and 859 cm^{-1} of the TP-2.45 sample, see Fig. 6a. Interestingly, if there is a phase transformation from anatase to rutile, characteristic peaks of rutile [13] (235, 445 and 612 cm^{-1}) shall appear. Judging from the results in Fig. 6a, we conclude that there is no rutile phase in the studied four samples. Therefore, the new Raman peaks at 231, 285, 460 and 859 cm^{-1} are attributed to the possible formation of a new potassium titanate compound. Such hypothesis is supported by the literature where similar peaks have been identified from $K_2Ti_2O_5$ and $K_2Ti_6O_{13}$ [19]. The DFT calculations in Fig. 7 also support the formation of a potassium titanate structure. We also note that while a trace of potassium oxide was applied to TiO_2 samples, it took a longer time (~10 s) to detect new Raman peaks. Meanwhile, the prolonged collecting time resulted in very strong intensities of characteristic anatase Raman peaks at 141, 393, 514, 635 cm^{-1}, as shown in Fig. 6a. Those peak intensities were beyond the detecting limit of the equipment, therefore were interpreted as plateaus. On the other hand, Fig. S6 in the Supporting Information was reported to show the four characteristic anatase peaks, collected at a typical time window of 1 s. We note that it is challenging to distinguish details of possible new crystal phases. This is because there are many potassium titanates and each has complex Raman spectra. Also, results in Fig. 6b reveal that the Raman signal (1630 cm^{-1}) of MB molecules decreases when the content of potassium increases. It suggests that a higher content of potassium significantly downgrades the Raman scattering performance.

The content and existence of interfacial trace potassium have been studied in other systems. Xie *et al.* reported that at high temperatures trace salts could disperse on oxide surfaces, spontaneously forming a monolayer [20,21]. In this work, it is hypothesized that trace potassium (0.5 wt%) disperses and stays at the surface of TiO_2 samples. By a simple sphere model, see Table S5 of the Supporting Information, we estimated the coverage of 0.5 wt% potassium on TiO_2 particles with different diameters. The analysis shows that when the diameter of TiO_2 particle is around 100 nm, which is similar to the size of TiO_2 nanowhiskers in this work, the atomic ratio of potassium/titanium at TiO_2 surface is around 1. Such analysis suggests that the 0.5 wt% of potassium might

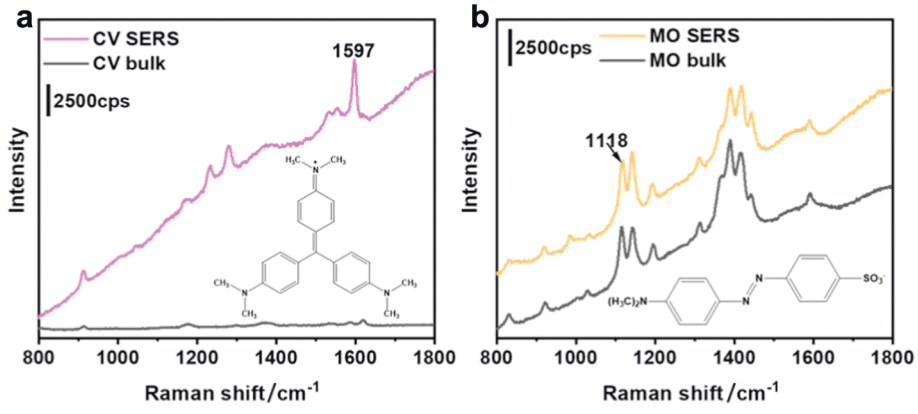

Fig. 5. Comparing Raman spectra of bulk dye and SERS spectra of 10^{-5} mol·L^{-1} dye solution adsorbed on Z700. (a Crystal violet, insert: CV structure; b Methyl orange, insert: MO structure.)

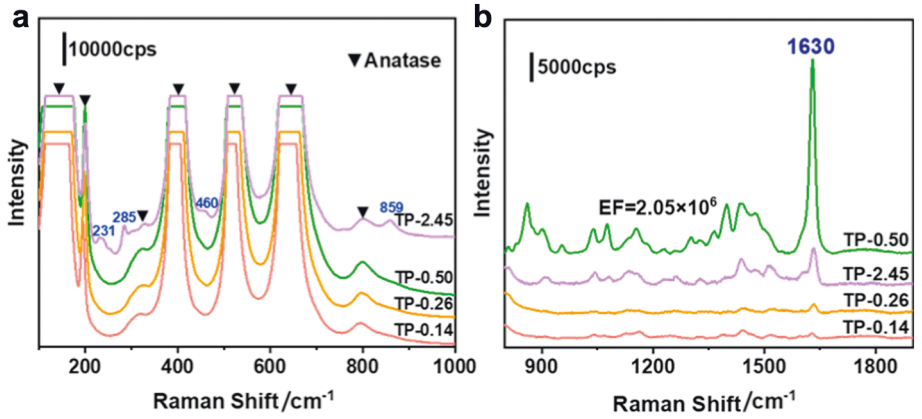

Fig. 6. Potassium treated TiO_2 particles and their SERS performance. (a) Raman spectra of commercial TiO_2 particles doped with different content of potassium (0.14, 0.26, 0.50 and 2.45 wt %) and (b) SERS spectra of MB (10^{-5} mol·L^{-1}) on TiO_2 particles.

form a thin layer at the surface of TiO_2 samples and show the best SERS performance.

In order to further understand the interaction between potassium and TiO_2 surface, as well as the potassium/TiO_2 structural information at elevated temperatures, a series of *ab initio* density functional theory (DFT) calculations and *ab initio* molecular dynamics (AIMD) simulations have been performed *via* Vienna *Ab initio* Simulation Package (VASP) of the MedeA computational platform [22]. The ion-electron interactions were described through the projector-augmented wave (PAW) method [23], with the electrons from Ti-pv ($3p^6 3d^2 4s^2$), O ($2s^2 2p^4$) and K-pv ($3p^6 4s^1$). The electron exchange and correlation interactions were represented by generalized gradient approximation (GGA) of Perdew–Burke–Ernzerhof (PBE) functionals [24]. Van der Waals interactions were described through Grimme's DFT-D3 semi-empirical method [25]. A cutoff energy of 450 eV was adopted for the planewave basis set and all calculations were performed using a Gaussian smearing with a width of 0.2 eV. The ionic relaxation is considered converged when the atomic force is smaller than 0.2 eV·nm^{-1}. Self-consistent field (SCF) cycles would stop when successive energy difference is less than 10^{-5} eV.

As shown in Fig. 7a, we generated a K-coated TiO_2 model *via* K_2O dissociative adsorption at the anatase (001) surface. The initial configuration was constructed by placing a 2×2 K_2O (001) supercell on top of a 4-layer anatase (001) surface. The anatase (001) surface model had the size of a = b = 1.145 nm, c = 0.950 nm, and a vacuum of 1.5 nm was added to avoid the interactions between periodic images. During the calculations, the bottom 2 layers were fixed to mimic the bulk behaviour, and all other parts were allowed to relax. It is worth noting that the size of the 2×2 K_2O (001) supercell was chosen based on the experimental K/Ti ratio of about 1.0. With our K_2O/TiO_2 model, the interfacial K/Ti is 8/9. Fig. 7b shows the equilibrium structure at 300 K, where eight potassium distribute nicely at the interface and each form two bonds with neighboring oxygen sites. For the interfacial oxygens, 4 were from the K_2O supercell and a few Ti—O bonds would break during the structural optimization to form interfacial K—O bonds. Other than that, there is a negligible TiO_2 structural change due to K_2O adsorption, which confirms the XRD results shown in Fig. 2b. Thermal stability of the K-coated TiO_2 model has been also tested, as illustrated in Fig. 7c, the structure remains stable even at 1000 K. No structural transition was observed for the anatase (001) surface, which is likely due to the

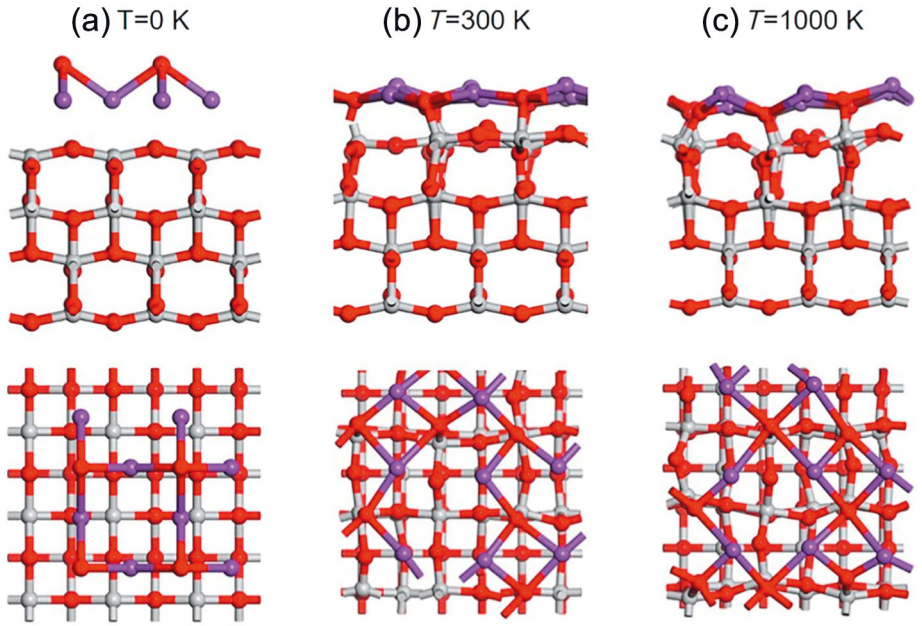

Fig. 7. The K-coated TiO_2 model *via* K_2O dissociative adsorption at the anatase (001) surface. (a) side and top views of the initial configuration, where a 2×2 K_2O (001) supercell is placed on top of a 4-layer anatase (001) surface; (b) side and top views of the equilibrium K-coated TiO_2 model at 300 K; (c) side and top views of the equilibrium K-coated TiO_2 model at 1000 K. The model has a good thermo stability, due to the stable K/O structure formed at the interface. Color code: purple, potassium; red, oxygen; gray, titanium.

stable K/O structure formed at the interface. The excellent thermo stability also explains why the synthesized TiO_2 nanowhisker has a good crystallinity under elevated temperatures up to 900 °C.

The surface charge information was also studied *via* the Bader charge analysis method [26]. As illustrated in Fig. 8, the interfacial K and O sites were labeled with respective atomic charges. Our calculation agrees with previous DFT results that interfacial potassium would transfer about one electron to neighboring oxygen sites, therefore carries a positive charge [27]. The summation of all interfacial K and O sites produces an overall negative charge of ~1.3046 e. The Bader charge analysis explains the Zeta potential measurements in Fig. 4f, and also supports the experimental hypothesis that the K-coated TiO_2 nanowhisker has a negative surface charge, therefore favors specific adsorptions of MB and CV molecules *via* their positively charged groups.

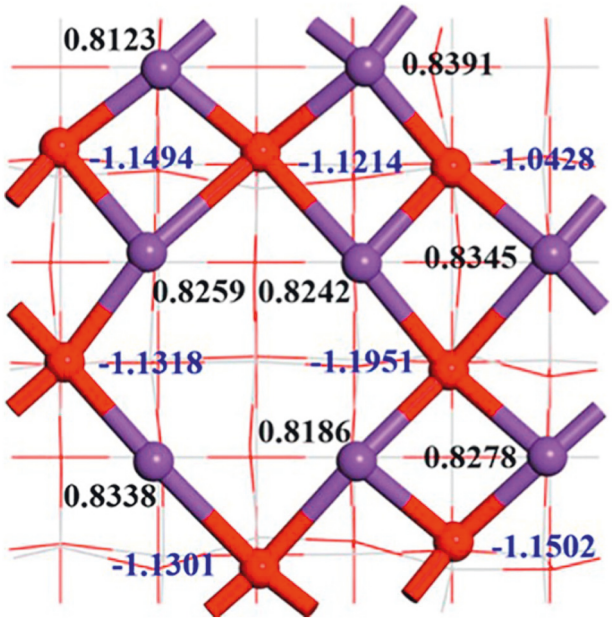

Fig. 8. Bader charge analysis for the interfacial potassium and oxygen sites: potassium carries a positive while the oxygen sites have negative charges. For charity, only the interfacial charge information is displayed. The bottom TiO_2 structures is shown by a line model and the charge information is not shown. Color code: purple, potassium; red, oxygen.

4. Conclusions

In summary, TiO_2 nanowhiskers have been synthesized with excellent surface enhanced Raman spectroscopy properties towards molecules with positive charge groups such as methylene blue and crystal violet. By a combination of experimental characterizations and computational studies, we reveal that the single-layer coated potassium at the TiO_2 nanowhisker helps to achieve a high thermo stability, which in return enables a high crystallinity at elevated temperatures up to 900 °C. In addition, Zeta potential measurements and theoretical Bader charge analysis show that the K-coated nanowhisker carries negative surface charges, which favors specific adsorptions of methylene blue molecules, and promotes the SERS enhancement factor, an index of SERS performance, to be about 4.96×10^6 and a detection limit around 10^{-7} mol·L^{-1}.

Acknowledgements

This work was supported by National Natural Science Foundation of China (21878143, 21476106, and 21838004), Joint Research Fund for Overseas Chinese Scholars and Scholars in Hong Kong and Macao Young Scholars (21729601), the fund of State Key Laboratory of Materials-Oriented Chemical Engineering (ZK201702, KL16-01), the Priority Academic Program Development of Jiangsu Higher Education Institutions (PAPD). Zhou and Huang acknowledge the U.S. National Science Foundation (NSF) for support through Grant No. CHE-1710102. We are grateful to the High-Performance Computing Center of Nanjing Tech University for supporting the computational resources.

Supplementary Material

Supplementary data to this article can be found online at https://doi.org/10.1016/j.cjche.2019.10.003.

References

[1] C. Zong, M. Xu, L. Xu, T. Wei, X. Ma, X. Zheng, R. Hu, B. Ren, Surface-enhanced Raman spectroscopy for bioanalysis: Reliability and challenges, *Chem. Rev.* 118 (2018) 4946–4980.
[2] X. Yan, Y. Xu, B. Tian, J. Lei, J. Zhang, L. Wang, Operando SERS self-monitoring photocatalytic oxidation of aminophenol on TiO_2 semiconductor, *Appl. Catal. B Environ.* 224 (2018) 305–309.
[3] J. Yu, J. Lei, L. Wang, J. Zhang, Y. Liu, TiO_2 inverse opal photonic crystals: Synthesis, modification, and applications-a review, *J. Alloy. Compd.* 769 (2018) 740–757.
[4] I. Alessandri, J.R. Lombardi, Enhanced Raman scattering with dielectrics, *Chem. Rev.* 116 (2016) 14921–14981.
[5] L. Yang, Y. Peng, Y. Yang, J. Liu, Z. Li, Y. Ma, Z. Zhang, Y. Wei, S. Li, Z. Huang, Green and sensitive flexible semiconductor SERS substrates: Hydrogenated black TiO_2 nanowires, *ACS Appl. Nano Mater.* 1 (2018) 4516–4527.
[6] I. Alessandri, Enhancing Raman scattering without plasmons: Unprecedented sensitivity achieved by TiO_2 shell-based resonators, *J. Am. Chem. Soc.* 135 (2013) 5541–5544.
[7] D. Qi, L. Lu, L. Wang, J. Zhang, Improved SERS sensitivity on plasmon-free TiO_2 photonic microarray by enhancing light-matter coupling, *J. Am. Chem. Soc.* 136 (2014) 9886–9889.
[8] L. Liu, F. Pan, C. Liu, L. Huang, W. Li, X. Lu, TiO_2 Nanofoam–nanotube Array for surface-enhanced Raman scattering, *ACS Appl, Nano Mater.* 1 (2018) 6563–6566.
[9] S. Cong, Y. Yuan, Z. Chen, J. Hou, M. Yang, Y. Su, Y. Zhang, L. Li, Q. Li, F. Geng, Noble metal-comparable SERS enhancement from semiconducting metal oxides by making oxygen vacancies, *Nat. Commun.* 6 (2015) 7800.
[10] J. Schneider, M. Matsuoka, M. Takeuchi, J. Zhang, Y. Horiuchi, M. Anpo, D.W. Bahnemann, Understanding TiO_2 photocatalysis: Mechanisms and materials, *Chem. Rev.* 114 (2014) 9919–9986.
[11] M. Gong, X. Jiang, J. Du, X. Li, X. Han, L. Yang, B. Zhao, Anatase TiO_2 nanoparticles with controllable crystallinity as a substrate for SERS: Improved charge-transfer contribution, *RSC Adv.* 5 (2015) 80269–80275.
[12] W. Li, Y. Bai, C. Liu, Z. Yang, X. Feng, X. Lu, N.K. van der Laak, K. Chan, Highly thermal stable and highly crystalline anatase TiO_2 for photocatalysis, *Environ. Sci. Technol.* 43 (2009) 5423–5428.
[13] J. Zhang, M. Li, Z. Feng, J. Chen, C. Li, UV Raman spectroscopic study on TiO_2. I. Phase transformation at the surface and in the bulk, *J. Phys. Chem. B* 110 (2006) 927–935.
[14] L. Yang, M. Gong, X. Jiang, D. Yin, X. Qin, B. Zhao, W. Ruan, Investigation on SERS of different phase structure TiO_2 nanoparticles, *J. Raman Spectrosc.* 46 (2015) 287–292.
[15] B. Dong, Y. Huang, N. Yu, Y. Fang, B. Cao, Y. Li, H. Xu, M. Sun, Local and remote charge-transfer-enhanced Raman scattering on one-dimensional transition-metal oxides, *Chem.-Asian J.* 5 (2010) 1824–1829.
[16] L. Yang, X. Jiang, W. Ruan, B. Zhao, W. Xu, J.R. Lombardi, Observation of enhanced Raman scattering for molecules adsorbed on TiO_2 nanoparticles: Charge-transfer contribution, *J. Phys. Chem. C* 112 (2008) 20095–20098.
[17] H. Hussain, G. Tocci, T. Woolcot, X. Torrelles, C.L. Pang, D.S. Humphrey, C.M. Yim, D.C. Grinter, G. Cabailh, O. Bikondoa, Structure of a model TiO_2 photocatalytic interface, *Nat. Mater.* 16 (2017) 461.
[18] J. Lin, Y. Shang, X. Li, J. Yu, X. Wang, L. Guo, Ultrasensitive SERS detection by defect engineering on single Cu_2O superstructure particle, *Adv. Mater.* 29 (2017) 1604797.
[19] C.E. Bamberger, G.M. Begun, C.S. Macdougall, Raman spectroscopy of potassium titanate: Their synthesis, hydrolytic reactions, and thermal stability, *Appl. Spectrosc.* 44 (1990) 30–37.
[20] X. Yu, N. Wu, Y. Xie, Y. Tang, A monolayer dispersion study of titania-supported copper oxide, *J. Mater. Chem.* 10 (2000) 1629–1634.
[21] C. Lin, X. Cai, Y. Xie, Study of dispersion state of $CuCl_2$ onto the surface of NaY zeolite, *Acta Phys. -Chim. Sin.* 12 (1996) 523–526.
[22] G. Kresse, J. Furthmüller, Efficient iterative schemes for ab initio total-energy calculations using a plane-wave basis set, *Phys. Rev. B* 54 (1996) 11169.
[23] P.E. Blöchl, Projector augmented-wave method, *Phys. Rev. B* 50 (1994) 17953.
[24] J.P. Perdew, K. Burke, M. Ernzerhof, Generalized gradient approximation made simple, *Phys. Rev. Lett.* 77 (1996) 3865.
[25] S. Grimme, J. Antony, S. Ehrlich, H. Krieg, A consistent and accurate ab initio parametrization of density functional dispersion correction (DFT-D) for the 94 elements H-Pu, *J. Chem. Phys.* 132 (2010) 154104.
[26] R. Bader, Atoms in molecule, A Quantum Theory, Oxford University Press, UK, 1990.
[27] M. Calatayud, C. Minot, Effect of alkali doping on a V_2O_5/TiO_2 catalyst from periodic DFT calculations, *J. Phys. Chem. C* 111 (2007) 6411–6417.